

Dynamics of binary black holes in low-mass young star clusters

Sara Rastello^{1,2*}, Michela Mapelli^{1,2,3†}, Ugo N. Di Carlo^{1,2,3}, Giuliano Iorio^{1,2,3},
Alessandro Ballone^{1,2,3}, Nicola Giacobbo^{1,4}, Filippo Santoliquido^{1,2}, Stefano Torniamenti^{1,2,3}

¹Physics and Astronomy Department Galileo Galilei, University of Padova, Vicolo dell'Osservatorio 3, I-35122 Padova, Italy

²INFN - Padova, Via Marzolo 8, I-35131 Padova, Italy

³INAF - Osservatorio Astronomico di Padova, Vicolo dell'Osservatorio 5, I-35122 Padova, Italy

⁴School of Physics and Astronomy, Institute for Gravitational Wave Astronomy, University of Birmingham, Birmingham, B15 2TT, UK

Accepted XXX. Received YYY; in original form ZZZ

ABSTRACT

Young star clusters are dynamically active stellar systems and are a common birthplace for massive stars. Low-mass star clusters ($\sim 300 - 10^3 M_\odot$) are more numerous than massive systems and are characterized by a two-body relaxation time scale of a few Myr: the most massive stars sink to the cluster core and dynamically interact with each other even before they give birth to compact objects. Here, we explore the properties of black holes (BHs) and binary black holes (BBHs) formed in low-mass young star clusters, by means of a suite of 10^5 direct N -body simulations with a high original binary fraction (100% for stars with mass $> 5 M_\odot$). Most BHs are ejected in the first ~ 20 Myr by dynamical interactions. Dynamical exchanges are the main formation channel of BBHs, accounting for $\sim 40 - 80\%$ of all the systems. Most BBH mergers in low-mass young star clusters involve primary BHs with mass $< 40 M_\odot$ and low mass ratios are extremely more common than in the field. Comparing our data with those of more massive star clusters ($10^3 - 3 \times 10^4 M_\odot$), we find a strong dependence of the percentage of exchanged BBHs on the mass of the host star cluster. In contrast, our results show just a mild correlation between the mass of the host star cluster and the efficiency of BBH mergers.

Key words: stars: black holes – black hole physics – Galaxy: open clusters and associations: general – stars: kinematics and dynamics – gravitational waves

1 INTRODUCTION

The number of gravitational-wave (GW) events observed by the LIGO–Virgo collaboration (LVC, Aasi et al. 2015; Acernese et al. 2015) has already grown to several dozens. In particular, the second GW transient catalogue (GWTC-2, Abbott et al. 2020b,d,e) consists of 50 candidate compact binary mergers: 3 from the first observing run (O1, Abbott et al. 2016b; Abbott et al. 2016c,a), 8 from the second (O2, Abbott et al. 2019a; Abbott et al. 2019b) and 39 from the first half of the third observing run (O3a).

Most events in GWTC-2 are associated with binary black hole (BBH) mergers with component masses ranging between ~ 5 and $\sim 90 M_\odot$. GWTC-2 also includes the most massive binary merger observed to date, GW190521 (Abbott et al. 2020f,h). In this case, the merger of two massive black holes (BHs, $\approx 85 M_\odot$ and $\approx 66 M_\odot$) resulted in the formation of a BH remnant of $\approx 142 M_\odot$ providing the first clear detection of an intermediate-mass BH in the $100 - 1000 M_\odot$ range (Abbott et al. 2020e; Abbott et al. 2020i; Nitz & Wang 2021; Fishbach & Holz 2020). In addition, O3a witnessed the first observation of a BBH with asymmetric masses (GW190412, Abbott et al. 2020a), and the second binary neutron star merger (GW190425, Abbott et al. 2020g). Finally, GW190814 might be the first BH–

neutron star binary merger, with masses ≈ 23 and $\approx 2.6 M_\odot$: its secondary component is either the lighter BH or the most massive neutron star ever observed.

This wealth of GW observations opens a new window on the study of BBHs. As pointed out by various authors (Fishbach et al. 2017; Zevin et al. 2017; Stevenson et al. 2017; Farr et al. 2017; Vitale et al. 2017; Gerosa & Berti 2017; Gerosa et al. 2018; Bouffanais et al. 2019, 2020, 2021; Wong & Gerosa 2019; Wong et al. 2021a; Zevin et al. 2020; Doctor et al. 2020; Kimball et al. 2020; Ng et al. 2020), a few hundreds of GW detections might be sufficient to disentangle the main formation pathways of BBHs, such as isolated binary evolution and dynamical assembly. On the one hand, the evolution of massive isolated stellar binaries can lead to the formation of tight BBHs either via common envelope (e.g. Tutukov & Yungelson 1973; Bethe & Brown 1998; Portegies Zwart & Yungelson 1998; Belczynski et al. 2002, 2008, 2010; Dominik et al. 2012, 2013; Mennekens & Vanbeveren 2014; Belczynski et al. 2016; Loeb 2016; Belczynski et al. 2016; de Mink & Mandel 2016a; Marchant et al. 2016a; Mapelli & Giacobbo 2018; Mapelli et al. 2019; Giacobbo & Mapelli 2018; Kruckow et al. 2018; Spera et al. 2019; Tang et al. 2020; Belczynski et al. 2020; García et al. 2021), via chemically homogeneous evolution (de Mink & Mandel 2016b; Mandel & de Mink 2016; Marchant et al. 2016b; du Buisson et al. 2020), or via stable mass transfer (e.g., Giacobbo et al. 2018; Neijssel et al. 2019; Bavera et al. 2021). On the other hand, dynamical interactions can trigger the formation

* E-mail: sara.rastello@unipd.it

† E-mail: michela.mapelli@unipd.it

of BBHs in dense stellar systems such as globular clusters (GCs, e.g., Downing et al. 2010; Benacquista & Downing 2013; Rodriguez et al. 2015, 2016a; Antonini & Rasio 2016; Askar et al. 2017; Fujii et al. 2017; Askar et al. 2018; Fragione & Kocsis 2018; Rodriguez et al. 2019), nuclear star clusters (e.g., O’Leary et al. 2009; Miller & Lauburg 2009; McKernan et al. 2012; Arca-Sedda & Capuzzo-Dolcetta 2018; McKernan et al. 2018; VanLandingham et al. 2016; Stone et al. 2017; Hoang et al. 2018; Arca-Sedda & Gualandris 2018; Antonini et al. 2019; Arca Sedda & Mastrobuono-Battisti 2019; Arca Sedda et al. 2020; Mapelli et al. 2021) and young massive star clusters (YSCs, e.g., Portegies Zwart & McMillan 2002; Banerjee et al. 2010; Mapelli et al. 2013; Ziosi et al. 2014; Goswami et al. 2014; Mapelli 2016; Banerjee 2017, 2018; Rastello et al. 2019; Perna et al. 2019; Di Carlo et al. 2019; Kumamoto et al. 2019, 2020; Rastello et al. 2020a; Banerjee 2021a). Dynamical mergers can also be the result of (triple-multiple) hierarchical systems in the field (e.g., Antonini et al. 2017; Silsbee & Tremaine 2017; Fragione et al. 2018; Fragione & Loeb 2019a,b; Fragione et al. 2020) or gas-assisted hierarchical assembly in AGN discs (e.g., McKernan et al. 2012, 2018; Bartos et al. 2017; Yang et al. 2019; Tagawa et al. 2020).

Isolated binary evolution predicts the formation of BBHs with preferentially equal-mass systems, mostly aligned spins and zero eccentricity in the LVC band (Mandel & de Mink 2016; Gerosa et al. 2018, but see Stegmann & Antonini 2021 for a possible spin flip mechanism). In contrast, the dynamical formation in star clusters might lead to even larger primary masses (e.g. McKernan et al. 2012; Mapelli 2016; Antonini & Rasio 2016; Gerosa & Berti 2017; Stone et al. 2017; McKernan et al. 2018; Di Carlo et al. 2020b; Rodriguez et al. 2019; Yang et al. 2019; Arca Sedda & Mastrobuono-Battisti 2019; Arca Sedda et al. 2020), mass ratios ranging from $q \sim 0.1$ to $q \sim 1$ (e.g. Di Carlo et al. 2019), isotropic spin distribution (e.g., Rodriguez et al. 2016b), and, in some rare but not negligible cases, non-zero eccentricity in the LVC band (e.g., Samsing 2018; Samsing & D’Orazio 2018; Samsing et al. 2018; Rodriguez et al. 2018; Zevin et al. 2019).

Here, we study the formation and evolution of BBHs in extremely low-mass young star clusters (YSCs, $300 < m_{\text{SC}} < 1000 M_{\odot}$). Such small star clusters are significantly more numerous than the massive ones, given the slope of the star cluster mass function ($dN/dm_{\text{SC}} \propto m_{\text{SC}}^{-2}$, Portegies Zwart et al. 2010; Fujii & Portegies Zwart 2016), but have frequently been overlooked in the study of binary compact objects.

In star clusters, dynamical evolution is driven by two-body relaxation, which proceeds over a timescale (Binney & Tremaine 2008)

$$t_{\text{rlx}} \sim 6 \text{ Myr} \left(\frac{m_{\text{SC}}}{1000 M_{\odot}} \right)^{1/2} \left(\frac{r_{\text{h}}}{1 \text{ pc}} \right)^{3/2} \left(\frac{\langle m \rangle}{1 M_{\odot}} \right)^{-1}, \quad (1)$$

where r_{h} is the cluster half mass radius and $\langle m \rangle$ is the average mass of a star in the cluster. For low-mass young star clusters, t_{rlx} ranges between a few Myr and ≈ 10 Myr, while for massive star clusters, such as globular and nuclear star clusters, t_{rlx} is of the order of several hundred Myr.

Since the dynamical friction time for a star with mass m scales as $t_{\text{DF}} \propto t_{\text{rlx}} \langle m \rangle / m$ (Chandrasekhar 1943), massive stars usually die before they can sink to the centre of a globular/nuclear star cluster, while they can reach the core of a low-mass YSC before they collapse to BH (Portegies Zwart & McMillan 2000). Hence, mass segregation is extremely efficient in low-mass YSCs, leading to frequent dynamical interactions between massive stars in the first Myrs (e.g., Portegies Zwart & McMillan 2002; Fujii & Portegies Zwart 2014): the stellar progenitors of BHs and neutron stars can even collide with each other in the core of a low-mass YSC, before

collapsing to compact objects (e.g., Kumamoto et al. 2019; Di Carlo et al. 2019).

Given the low velocity dispersion of YSCs (just a few km s^{-1} , Spitzer 1987a; Portegies Zwart et al. 2010; Rastello et al. 2020b), most binary stars are hard (i.e., they have binding energy larger than the average kinetic energy of a cluster star, Heggie 1975) in such environments. This implies that almost all the original binary stars survive in a small YSC, while in nuclear star clusters most binaries are soft and get disrupted by encounters. Hence, dynamical exchanges involving original binaries are favoured in low-mass YSCs with respect to more massive clusters. For these reasons, the dynamical processes affecting their stellar progenitors (e.g., mass segregation, stellar collisions and dynamical exchanges) play a more important role for the formation of BBHs in low-mass YSCs than in more massive clusters.

Another peculiarity of these systems is that each cluster hosts a few BH and neutron star progenitors ($\sim 1 - 6$ for star clusters with mass $\sim 300 - 1000 M_{\odot}$). This favours the pair up of BH–neutron star systems with respect to more massive clusters (Rastello et al. 2020a). Low-mass YSCs are extremely clumpy and asymmetric stellar systems (Ballone et al. 2020), almost impossible to model with Monte Carlo codes, which are based on the assumption of spherical symmetry (Hénon 1960). Moreover, stellar and binary evolution are a key ingredient in the life of YSCs. Since they evolve on timescales comparable to the lifetime of their massive stars (eq. 1), mass loss by supernova (SN) explosions and by stellar winds contribute significantly to their dynamical evolution (Mapelli & Bressan 2013; Trani et al. 2014). Hence, in order to model low-mass YSCs, we have to run expensive direct N -body simulations coupled with binary population-synthesis codes.

Here, we make use of the dynamical code NBODY6++GPU (Wang et al. 2015, 2016), coupled with MOBSE (Mapelli et al. 2017; Giacobbo et al. 2018).

2 METHODS

2.1 Numerical Codes

We performed a suite of N -body simulations using the direct-summation N -body code NBODY6++GPU (Wang et al. 2015). In particular, we adopted the same version of the code as described in Di Carlo et al. (2019).

NBODY6++GPU is the GPU parallel version of NBODY6 (Aarseth 2003). It implements a 4th-order Hermite integrator, individual block time-steps (Makino & Aarseth 1992) and Kustaanheimo-Stiefel regularization of close encounters and few-body systems (Stiefel 1965; Mikkola & Aarseth 1993). Post-Newtonian terms are not included in the version of the code we used. A neighbour scheme (Nitadori & Aarseth 2012) is used to compute the force contributions at short time steps (*irregular* force/timesteps) while for longer time steps (*regular* force/timesteps) all the members of the system are included when evaluating the force. The regular forces are computed on GPUs using the CUDA architectures while irregular forces are evaluated using CPUs.

In our simulations, NBODY6++GPU is interfaced with the binary population synthesis code MOBSE (Mapelli et al. 2017; Giacobbo et al. 2018; Giacobbo & Mapelli 2018), which is an upgrade of BSE (Hurley et al. 2000, 2002), including up-to-date prescriptions for stellar winds, electron capture, pair instability, pulsational pair instability and core-collapse SNe. Mass loss by stellar winds is described as $\dot{M} \propto Z^{\beta}$ for all hot massive stars. The index β is a function of the electron-scattering Eddington ratio, accounting for the increase of the

mass-loss rate when a star is close to its Eddington limit (Gräfenor & Hamann 2008; Chen et al. 2015).

We adopt the rapid core-collapse SN model (Fryer et al. 2012), which prevents the formation of compact objects with mass in the range $2 - 5 M_{\odot}$. Electron capture SNe are modelled as described in Giacobbo & Mapelli (2019), while (pulsational) pair instability SNe follow the formalism presented in Spera & Mapelli (2017) and Mapelli et al. (2020). This setup produces a mass gap in the BH mass spectrum between $m_{\text{BH}} \sim 65 M_{\odot}$ and $m_{\text{BH}} \sim 120 M_{\odot}$.

Binary evolution processes, such as tides, mass transfer, common envelope and GW orbital decay, are implemented as in Hurley et al. (2002). For common envelope, we adopt the energy formalism (Webbink 1984), assuming $\alpha = 5$, while the concentration parameter λ is calculated self-consistently as described in Claeys et al. (2014).

Natal kicks are randomly drawn from a Maxwellian velocity distribution with a one-dimensional root mean square velocity $\sigma = 15 \text{ km s}^{-1}$ (Giacobbo & Mapelli 2018). For BHs, we also modulate the kick magnitude by the amount of fallback, as described in Fryer et al. (2012). When two stars merge, the amount of mass loss is decided by the population synthesis code MOBSE, which adopts the same prescriptions as BSE. If a star merges with a neutron star or a BH, the mass of the star is immediately lost by the merger product and there is no mass accretion on the compact object (Giacobbo et al. 2018).

2.2 Initial Conditions

We explore three different metallicities: $Z = 0.02, 0.002$ and 0.0002 . We ran 33334 direct N -body simulations per each metallicity for a total of 100002 simulations. The YSCs studied in this work have masses sampled in the range $300 \leq m_{\text{SC}}/M_{\odot} < 1000$ from a power-law distribution $dN/dm_{\text{SC}} \propto m_{\text{SC}}^{-2}$, reminiscent of the distribution of YSCs in Milky-Way like galaxies (Lada & Lada 2003).

The initial star cluster half mass radius r_h is chosen according to Marks & Kroupa (2012):

$$r_h = 0.10^{+0.07}_{-0.04} \text{ pc} \left(\frac{m_{\text{SC}}}{M_{\odot}} \right)^{0.13 \pm 0.04}. \quad (2)$$

Our YSCs are initially set with $q_{\text{vir}} = T/|V| = 0.5$ (where T and V are the total kinetic and potential energy of the YSC, respectively) and are modelled with fractal substructures, to account for the initial clumpiness and asymmetry of YSCs (Goodwin & Whitworth 2004). We choose a fractal dimension $D = 1.6$, as suggested by observations (Sánchez & Alfaro 2009; Küpper et al. 2011b; Kuhn et al. 2019) and hydrodynamical simulations (Ballone et al. 2020). We generated these initial conditions using the code MCLUSTER (Küpper et al. 2011a).

Stellar masses are extracted from a Kroupa (Kroupa 2001) initial mass function (IMF) in the range $0.1 \leq m \leq 150 M_{\odot}$. We draw the orbital parameters of original binaries following the distributions by Sana et al. (2012). In particular, orbital periods P follow the distribution $\mathcal{P}(\Pi) \propto \Pi^{-0.55}$, where $\Pi \equiv \log_{10}(P/\text{days})$ and $0.15 \leq \Pi \leq 6.7$, while binary eccentricities e are randomly drawn from a distribution $\mathcal{P}(e) \propto e^{-0.42}$ with $0 \leq e < 1$.

We assume that initially each YSC hosts a fraction $f_{\text{bin}} = 0.4$ of original binaries¹. MCLUSTER (Küpper et al. 2011a) assigns the companion stars based on mass: stars are randomly paired by using

a distribution $\mathcal{P}(q) \propto q^{-0.1}$, where $q = m_2/m_1$ is the ratio of the mass between the secondary and the primary star according to Sana et al. (2012). Hence, all the stars with mass $m \geq 5 M_{\odot}$ are members of binary systems, while stars with mass $m < 5 M_{\odot}$ are randomly paired until the imposed total binary fraction $f_{\text{bin}} = 0.4$ is reached. The result of this method is that the most massive stars (down to $5 M_{\odot}$) are all binary members, while the fraction of binaries falls to lower values for lighter stars, in agreement with Moe & Di Stefano (2017). We embed the simulated YSCs in a solar neighbourhood-like static external tidal field and we put them on a circular orbit around the centre of the Milky Way at a distance 8 kpc (Wang et al. 2016). The BBHs that escape from the cluster² evolve only due to the emission of gravitational radiation. We estimate the coalescence timescale of these binaries with the formalism described in Peters (1964). We integrate each YSC for a maximum time $t = 100 \text{ Myr}$.

As a result of the Kroupa IMF and of the formalism we adopted for BH formation, the total number of BHs per each star cluster follows a linear relation $n_{\text{BH}} = \mathcal{A} + \mathcal{B} (m_{\text{SC}}/M_{\odot})$, where $\mathcal{A} = 0.320 \pm 8 \times 10^{-3}$ and $\mathcal{B} = 0.003 \pm 1.5 \times 10^{-5}$, respectively. On average, the smallest YSCs ($m_{\text{SC}} \approx 300 M_{\odot}$) produce 1 BH, while the most massive systems we simulated ($m_{\text{SC}} \approx 1000 M_{\odot}$) produce up to 3 BHs. Hence, we can form just one BBH in each YSC, on average. This is another crucial difference with respect to more massive star clusters.

Throughout this paper, we compare our results with those described in Di Carlo et al. (2019) and Di Carlo et al. (2020b), who used the same code to study high-mass YSCs ($m_{\text{SC}} \in [10^3, 3 \times 10^4] M_{\odot}$).

Di Carlo et al. (2020b) explore two density regimes: i) dense YSCs, following the Marks et al. (2012) relation, with initial half-mass density $\rho_h \geq 3.4 \times 10^4 M_{\odot} \text{ pc}^{-3}$ (set A), and ii) loose YSCs, with initial half-mass radius $r_h = 1.5 \text{ pc}$ and initial half-mass density $\rho_h \geq 1.5 \times 10^2 M_{\odot} \text{ pc}^{-3}$ (set B). Our YSCs are the extension of set A of Di Carlo et al. (2020b) to low-mass systems.

Moreover, we compare our results to a set of isolated binaries simulated with MOBSE. This sample is composed of 3×10^7 binaries (10^7 for each metallicity). The primary masses of the isolated binaries are drawn from a Kroupa (Kroupa 2001) mass function between 5 and $150 M_{\odot}$. The initial orbital properties of the isolated binaries follow the same distributions as we described for original binaries in YSCs.

3 RESULTS

3.1 YSC Evolution

Figure 1 shows the global evolution of YSCs' main physical parameters: half mass radius r_h , core radius r_c (Casertano & Hut 1985) and stellar density ρ_h at the half-mass radius. Heavy YSCs ($700 < m_{\text{SC}}/M_{\odot} < 1000 M_{\odot}$) expand more slowly than lighter systems ($300 < m_{\text{SC}}/M_{\odot} < 700$), and the expansion is generally steeper in metal-poor than in metal-rich systems. In the initial conditions, all YSCs are tidally under-filling. Then, all the clusters expand and the smallest ones (in the mass range $300 - 700 M_{\odot}$) reach and exceed the tidal radius, becoming tidally over-filling. Only the most massive systems ($700 < m_{\text{SC}}/M_{\odot} < 1000$) remain tidally under-filling for the entire simulation. Hence, heavy clusters survive longer

¹ Here and in the following, *original binaries* are binary systems already present in the initial conditions.

² We define escapers as those stars and binaries that reach a distance from the centre of the YSC larger than twice the tidal radius, r_t , of the cluster (Aarseth 2012; Wang et al. 2015).

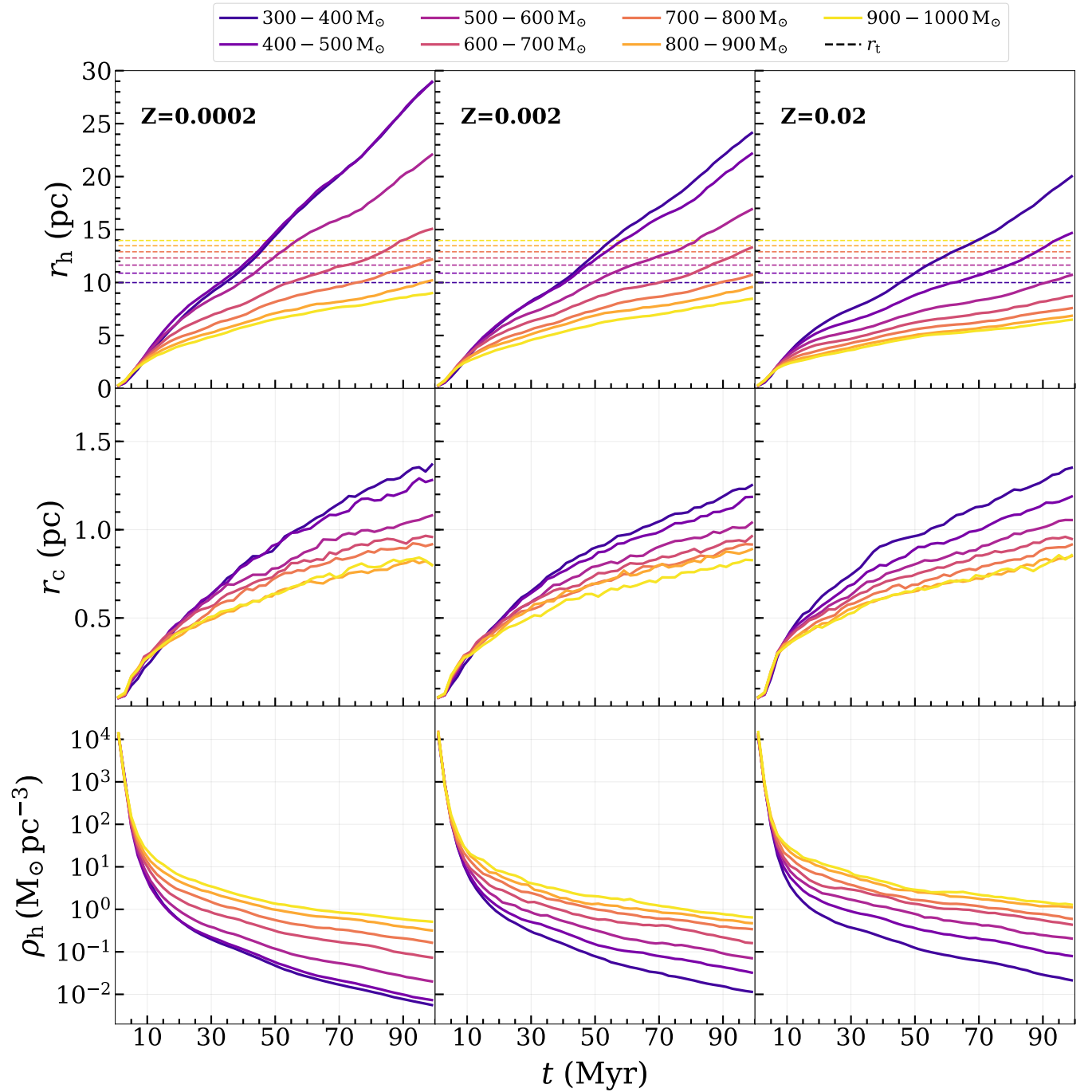


Figure 1. Half-mass radius r_h (solid lines in the upper panels), tidal radius r_t (dashed lines in the upper panels), core radius r_c (solid lines in the middle panel) and density at the half-mass radius ρ_h (solid lines in the lower panels) as a function of time. From left to right: metallicity $Z = 0.0002$, 0.002 and 0.02 , respectively. The various colours refer to different mass bins, corresponding to $m_{\text{SC}} \in [300, 400]$, $[400, 500]$, $[500, 600]$, $[600, 700]$, $[700, 800]$, $[800, 900]$ and $[900, 1000]$ M_\odot , respectively. Each line shows the median value over all the simulated YSCs, per each mass bin.

against the expansion, since they resist more efficiently the external tidal field.

As anticipated in Section 1, low-mass YSCs have extremely short relaxation time scale t_{rlx} , of the order of a few tens of Myr, and undergo core collapse over an even shorter time scale ($t_{\text{cc}} \approx 0.2 t_{\text{rlx}}$, Fujii & Portegies Zwart 2014). Our star clusters are essentially generated as already core-collapsed because of the high initial density of our models (Marks et al. 2012). The evolution of the core radius is thus a rapid expansion, which is rather faster in lighter systems.

After ~ 100 Myr, r_c has grown by a factor of ~ 28 (16) if $m_{\text{SC}} = 300$ ($m_{\text{SC}} = 1000 M_\odot$). The global evolution of the core radius is similar for each metallicity.

The initial rapid expansion of the clusters coincides with an initial drop of the density, which is initially $\rho_h \sim 10^4 M_\odot \text{pc}^{-3}$ and decreases to $\rho_h \sim 10^{-2} M_\odot \text{pc}^{-3}$ ($\rho_h \sim 1 M_\odot \text{pc}^{-3}$) at 100 Myr if $m_{\text{SC}} = 300 M_\odot$ ($m_{\text{SC}} = 1000 M_\odot$).

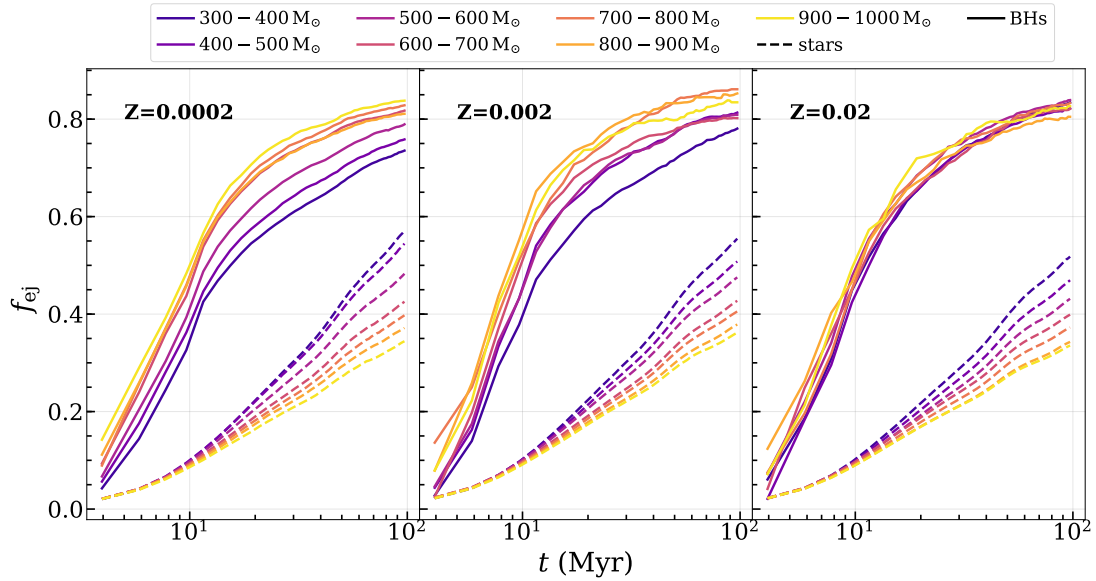


Figure 2. Solid (dashed) lines: fraction of ejected BHs (stars) with respect to the total number of BHs (stars). From left to right: $Z = 0.0002$, 0.002 and 0.02 . We adopt the same colour palette as in Figure 1.

3.2 Dynamical Ejection of BHs

Figure 2 shows the evolution of the fraction f_{ej} of ejected BHs with respect to all the BHs formed in each star cluster. For comparison, we also show the fraction of ejected stars over the whole cluster population. The fraction of ejected BHs increases with time, initially very fast and then, after ≈ 10 Myr, with a more gentle slope. The change of the slope approximately corresponds to the time at which all the BHs have formed and to the time at which the density has dropped by ~ 3 orders of magnitude (Figure 1). To draw Figure 2, we have considered only BHs after their formation: we have not included their progenitors. For this reason, the time shown in the x -axis should be regarded as the maximum between the time of ejection and the time of BH formation: several massive stars are ejected before they collapse to a BH.

Between 72 and 85% of all BHs are ejected from the star cluster by the end of the simulation. Moreover, even those BHs that remain inside the YSC spend most of their life in a low-density environment, given the drop of the density after ~ 10 Myr. Hence, the BHs formed in our YSCs undergo strong dynamical encounters and exchanges only up to a few $\times 10$ Myr, while BHs formed in globular clusters can undergo a long chain of exchanges and three-body encounters before being ejected.

If we look at the metal-poor star clusters ($Z = 0.0002, 0.002$), the fraction of ejected BHs is higher in the heavier YSCs than in the lighter ones, because the higher density of the heavier YSCs triggers more interactions and increases the chance to eject BHs via Spitzer instability (Spitzer 1987b).

This difference between lighter and heavier YSCs tends to disappear at solar metallicity, where the majority of BHs are relatively low-mass ($\sim 5 - 10 M_{\odot}$).

The fraction of ejected stars shows significant differences with respect to the one of BHs: after the first 10 Myr, the slope of the fraction of ejected stars becomes even steeper, while the fraction of ejected BHs becomes flatter. At the end of the simulations ~ 30 – 55% of the stars are ejected from their parent YSC. The lighter YSCs lose a higher fraction of stars than the heavier ones: at the end of the simulation, $f_{ej} \sim 0.5$ – 0.55 and ~ 0.30 – 0.35 in the YSCs with $m_{SC} \in$

$[300, 400] M_{\odot}$ and $m_{SC} \in [900, 1000] M_{\odot}$, respectively, with a very mild dependence on metallicity. This difference between BHs and stars reflects the different mechanism leading to their ejection. BHs are more massive than the average stellar mass, efficiently sink to the core by dynamical friction and are ejected by close dynamical encounters. In contrast, most of the ejected stars are light objects, populate the outskirts of their parent YSC and are tidally removed from it. The fraction of ejected stars is thus larger in the smaller YSCs, because these over-fill their tidal radius by the end of the simulation.

3.3 Exchanged versus Original BBHs

We label as *exchanged BBHs* those BBHs that form through dynamical exchanges or other kind of encounters, and we call *original BBHs* those BBHs that descend from the evolution of an original binary star (i.e. their stellar progenitors were already bound in the initial conditions). With the term *dynamical BBHs*, we indicate all the BBHs that evolve in YSCs, both original and exchanged. In fact, YSC dynamics affects not only exchanged binaries, but even original binaries: close dynamical encounters shrink (or widen) the semi-major axis of a binary system, change its eccentricity and can even break it. In general, lighter and wider binaries (soft binaries) tend to be widened/ionized, while massive and tight binaries (hard binaries) tend to increase their binding energy and shrink their orbit by close encounters (Heggie 1975).

Figure 3 shows the distribution of BBH masses as a function of star cluster mass and for different metallicities. The mass of both original and exchanged BBHs is mainly affected by the metallicity of the progenitors and does not depend on the mass of the host star cluster.

Exchanged BBHs are, on average, more massive than original BBHs: the median value of the mass of exchanged BBHs is ~ 80 , ~ 60 and $\sim 20 M_{\odot}$ at metallicity $Z = 0.0002, 0.002$ and 0.02 , respectively. In contrast, original BBHs are, on average, less massive (~ 60 , ~ 30 and $\sim 10 M_{\odot}$ at $Z = 0.0002, 0.002$ and 0.02 , respectively).

The percentage of original (exchanged) BBHs significantly de-

creases (increases) as the cluster mass increases. In fact, heavier clusters allow a larger number of dynamical encounters that tend to disrupt original binaries and to form more BBHs via exchanges.

BBHs in triple systems (also shown in Figure 3) form more frequently in metal-poor environments: 55 % (33%) of all BBHs are members of triple systems at $Z = 0.0002$ ($Z = 0.002$). At solar metallicity, only 10% of BBHs are in triples. The ratio between original and exchanged triples³ is quite balanced in metal-poor systems: at $Z = 0.0002$ ($Z = 0.002$), 49% (48%) of all BBHs in triples are exchanged systems. In contrast, at solar metallicity, the vast majority of BBHs in triples are original (80%).

Figure 4 shows the temporal evolution of the fraction of exchanged BBHs

$$f_{\text{exch}}(t) = \frac{N_{\text{exch}}(t)}{N_{\text{exch}}(100 \text{ Myr}) + N_{\text{orig}}(100 \text{ Myr})}, \quad (3)$$

where $N_{\text{exch}}(t)$ is the number of exchanged BBHs (or BBH progenitors) at each time step (t), while $N_{\text{exch}}(100 \text{ Myr})$ and $N_{\text{orig}}(100 \text{ Myr})$ are the number of exchanged and original BBHs at the end of our simulations ($t = 100 \text{ Myr}$). When calculating $N_{\text{exch}}(t)$ we consider not only BBHs that are already formed at time t , but also exchanges involving their stellar progenitors.

The fraction of exchanged BBHs has a fast growth in the first $\sim 10 \text{ Myr}$ and a shallower one in the next stages. This happens because exchanges are more efficient when the density is higher and figure 1 shows that the density drops at $\approx 10 \text{ Myr}$. Moreover, f_{exch} strongly depends on both YSC mass and metallicity. The heavier mass clusters are obviously more efficient in forming exchanged systems, because of their higher density and longer lifetime. For example, at $Z = 0.0002$, $f_{\text{exch}} \approx 0.55$ (≈ 0.75) in YSCs with mass $300 - 400 M_{\odot}$ ($900 - 1000 M_{\odot}$) at the end of the simulations.

Metal-poor YSCs ($Z = 0.0002, 0.002$) have higher values of f_{exch} than metal-rich ones. For example, at the end of the simulation, $f_{\text{exch}} \approx 0.55$ (≈ 0.35) in YSCs with mass $300 - 400 M_{\odot}$ at $Z = 0.0002$ ($Z = 0.02$). This difference springs from the dependence of BH mass on progenitor's metallicity: dynamical exchanges favour the formation of massive binaries, which are more energetically stable (e.g., Hills & Fullerton 1980); hence, massive BHs in metal-poor YSCs are more efficient in pairing up via exchanges.

Figure 5 shows the percentage of exchanged BBHs at the end of the simulation (P_{exch}) as a function of the star cluster mass m_{SC} . In this Figure, we include the YSCs from set A of Di Carlo et al. (2020b), which span from $m_{\text{SC}} = 10^3 M_{\odot}$ to $3 \times 10^4 M_{\odot}$. P_{exch} increases with the mass of the YSC. The percentage of exchanged BBHs increases from $\approx 60 \%$ in low-mass YSCs up to more than $\approx 90 \%$ in high-mass YSCs. Fitting the points in Fig. 5 with the linear fit $P_{\text{exch}} = a + b \log_{10}(m_{\text{SC}}/1000 M_{\odot})$, we obtain parameters $a = 65.1 \pm 3.1$ and $b = 18.9 \pm 0.2$. We also ran a Pearson's correlation test, to estimate the significance of the $P_{\text{exch}} - \log_{10} m_{\text{SC}}$ correlation. We obtain a Pearson's coefficient $r > 0.5$, implying a rather strong correlation between P_{exch} and m_{SC} . This correlation is steeper for metal-rich ($Z = 0.02$) than for metal-poor clusters ($Z = 0.0002$), possibly because in metal-poor environments original BBHs are more massive and more difficult to break by dynamical exchanges.

Massive YSCs, as those studied in Di Carlo et al. (2020b), have a larger probability to produce exchanged binaries because of the higher rate of dynamical encounters, which tend to destroy original binaries. In contrast, because of the fast dynamical evolution and the

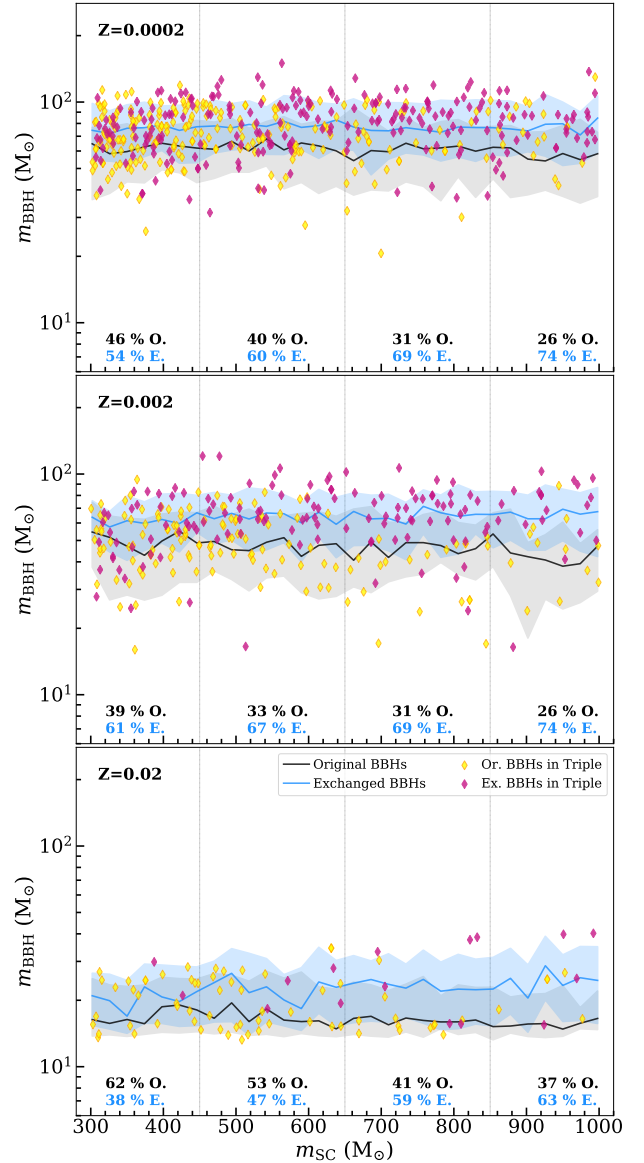


Figure 3. BBH total mass (m_{BBH}) as a function of the YSC mass (m_{SC}) at $Z = 0.0002, 0.002, 0.02$, (upper, middle and lower panel, respectively) at the end of the simulations (100 Myr). Solid lines indicate the median value of the BBH mass: blue for exchanged BBHs and black for original BBHs. The corresponding shaded areas (light blue and grey) indicate the confidence interval at the 20th and 80th percentile. Yellow and magenta diamonds indicate original and exchanged BBHs in triple systems, respectively. At each metallicity, we divide the YSCs into four bins of mass: $m_{\text{SC}} \in [300, 450] M_{\odot}$, $m_{\text{SC}} \in [450, 650] M_{\odot}$, $m_{\text{SC}} \in [650, 850] M_{\odot}$, and $m_{\text{SC}} \in [850, 1000] M_{\odot}$. The percentage of original (O.) and exchanged (E.) BBHs per each of these bins is reported in each panel.

rapid central density decrease, low-mass YSCs allow the survival of more original BBHs, while the formation of new binaries through dynamical exchanges is suppressed with respect to more massive clusters. Moreover, high-mass YSCs host more BHs (≈ 30 if $m_{\text{SC}} \approx 10^4 M_{\odot}$) than low-mass systems: a star cluster with $m_{\text{SC}} \approx 10^3 M_{\odot}$ hosts, on average, 3 BHs (see Section 2.2). Hence, a low-mass YSC may host at most one BBH plus, in a few cases, a single BH. Since massive stars tend to be part of binary systems with other massive stars (as a consequence of the algorithm we used to generate the initial conditions, which is supported by observations, see Section 2.2), in

³ In this case, we refer to the inner binary of the triple which may be an original or an exchanged BBH.

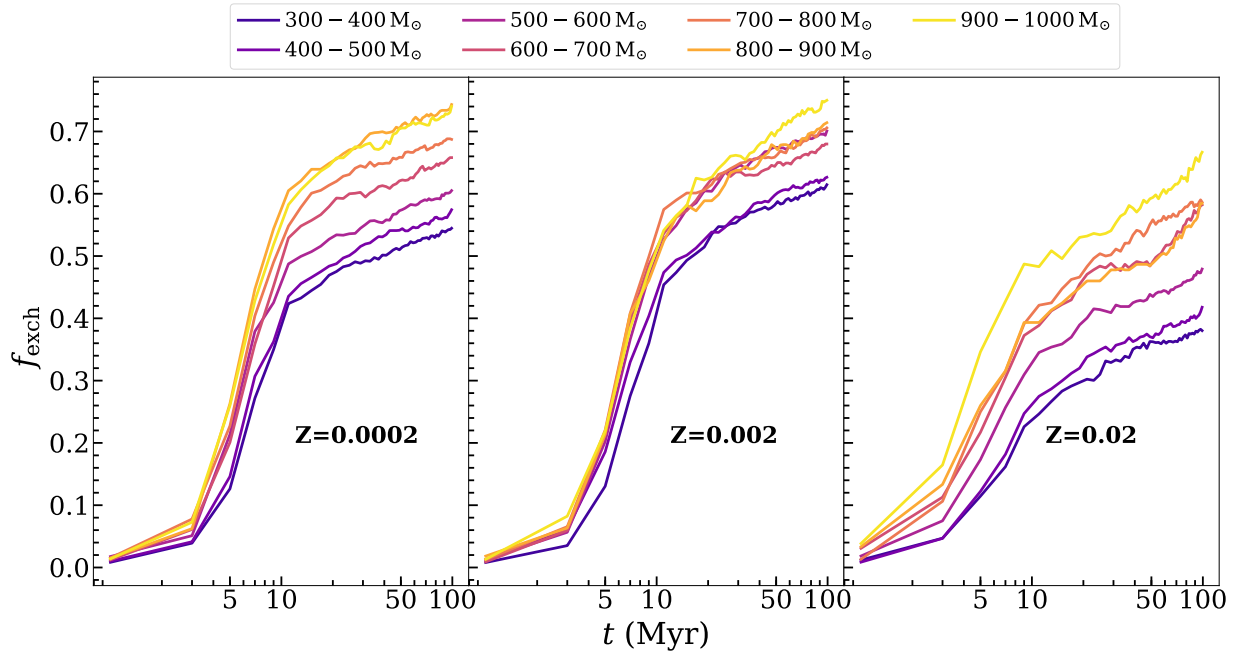


Figure 4. Evolution of the fraction of exchanged BBHs with respect to all BBHs at $Z = 0.0002$ (left), $Z = 0.002$ (middle) and $Z = 0.02$ (right). The colour map is the same as in Figure 1.

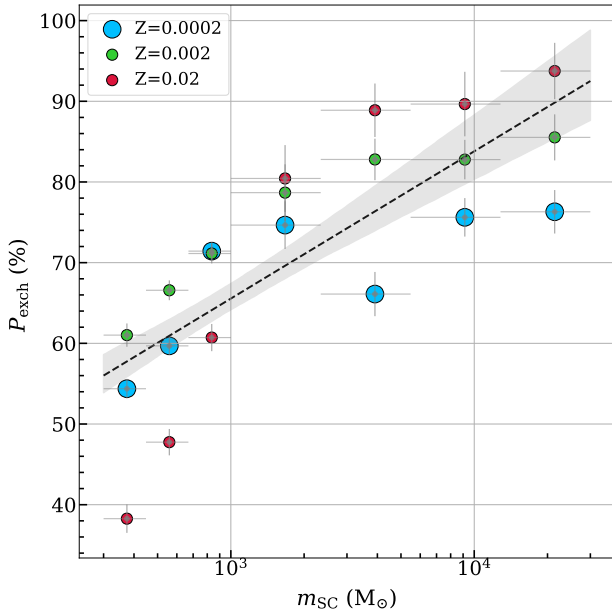


Figure 5. Percentage of exchanged BBHs (P_{exch}) per cluster mass bin (m_{SC}) in low-mass and high-mass YSCs. Blue, green and red points refer to $Z = 0.0002$, 0.002 and 0.02 , respectively. The error bars are Poissonian uncertainties. The black dashed line indicates the best linear fit (in the lin-log plane) and the grey bands refer to the confidence interval at the 20th and 80th percentile. The YSCs with $m_{\text{SC}} < 1000 M_{\odot}$ are from this work, while the YSCs with $m_{\text{SC}} \geq 1000 M_{\odot}$ are from Di Carlo et al. (2020b), set A.

the lowest mass clusters the only BBH tends to be the result of the evolution of the original binary composed of the two most massive stars. When there are no other BHs in the star cluster, it is extremely difficult that such a massive original binary undergoes an exchange, because the probability of an exchange is strongly suppressed if the intruders are less massive than the two members of the binary system

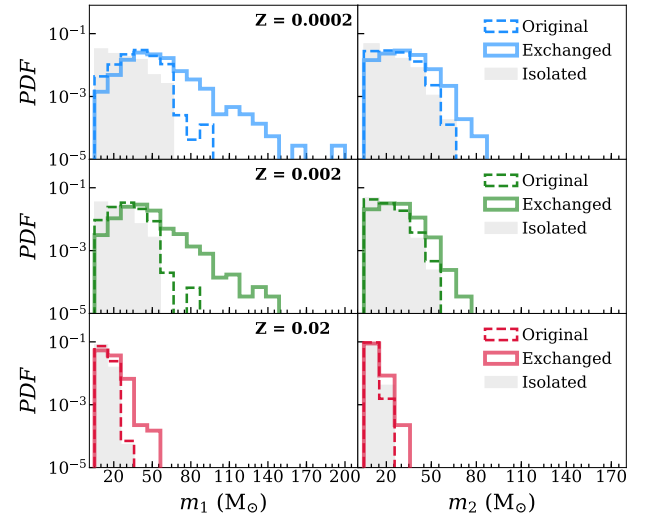


Figure 6. Mass of primary (m_1 , left panels) and secondary (m_2 , right panels) BHs of formed BBHs in YSCs and in isolation (filled grey histograms). The panels from top to bottom refer to the three metallicities: $Z = 0.0002$ (blue histogram), $Z = 0.002$ (green histogram) and $Z = 0.02$ (red histogram), respectively. Solid lines: exchanged BBHs; dashed lines: original BBHs.

(Hills & Fullerton 1980). For the same reason, low-mass YSCs favour the formation and merger of BH-neutron star binaries (Rastello et al. 2020a), which are, instead, highly suppressed in more massive star clusters (Ye et al. 2020).

3.4 Isolated vs Dynamical BBHs

We compare our dynamical BBHs with a set of *isolated BBHs*, that formed in the field from isolated binary evolution and that we evolved with `MOBSE` without dynamics. Figure 6 compares the mass distribution of BBHs formed in YSCs with that of BBHs formed in

isolation. This Figure shows both BBHs that merge within a Hubble time (hereafter, merging BBHs) and BBHs that are too loose to merge over the age of the Universe. The maximum mass of the primary components of exchanged BBHs, $m_{1,\text{max}}$, is significantly higher than that of original and isolated binaries, especially in metal-poor environments: at $Z = 0.0002$, $m_{1,\text{max}} \approx 197$, ≈ 91 and $\approx 63 M_{\odot}$ for exchanged, original and isolated BBHs, respectively. The most massive BHs in exchanged binaries originate from the merger of two (or more) stars, which then pair up dynamically (Portegies Zwart et al. 2004). Some of these masses are in the pair-instability mass gap (Di Carlo et al. 2020a). Light BBHs ($m_1 \lesssim 25 M_{\odot}$) are more common in isolated BBHs than in both original and exchanged BBHs, especially at low metallicity.

3.5 BBH Mergers

We now focus on merging BBHs, i.e. BBHs that reach coalescence within a Hubble time. In our dynamical simulations, we found ~ 430 merging BBHs. 60% of the merging BBHs are at metallicity $Z = 0.0002$, 35% at $Z = 0.002$ and 5% at $Z = 0.02$.

The percentage of original merging BBHs is always larger than that of exchanged binaries: $\approx 87\%$, $\approx 84\%$ and $\approx 95\%$ of merging BBHs are original at $Z = 0.0002$, 0.002 and 0.02 , respectively.

Merging BBHs follow the same trend we have already seen in Figure 5 for all (merging and non merging) BBHs: $\approx 90\%$ of the merging BBHs in low-mass YSCs ($300 - 10^3 M_{\odot}$) are original binaries, while in more massive systems (Di Carlo et al. 2020b) the percentage of original merging BBHs drops to $\approx 60\%$. However, when compared with Figure 5, these percentages indicate that original BBHs are more efficient in merging than exchanged BBHs. In fact, exchanged BBHs are $\sim 40 - 60\%$ ($\sim 80 - 90\%$) of all BBHs, but they represent only the $\sim 10\%$ ($\sim 40\%$) of the merging BBHs in the least massive YSCs (most massive YSCs). The reason is that exchanged BBHs generally form with larger semi-major axis than original BBHs and cannot shrink efficiently via dynamical encounters, especially in the least massive YSCs.

Figure 7 shows the total mass ($m_{\text{BBH}} \equiv m_1 + m_2$) of merging BBHs in YSCs and in isolation, while Figure 8 shows the mass of the primary (m_1) versus the mass of the secondary (m_2) BH component of merging BBHs in low-mass YSCs. Only two BBHs with primary mass $m_1 > 45 M_{\odot}$ are found in metal poor systems ($Z = 0.0002$), one is original and the other is an exchanged binary.

For comparison, Figure 9 shows the mass distribution of BBH mergers in low- ($300 - 10^3 M_{\odot}$) and high-mass YSCs ($10^3 - 3 \times 10^4 M_{\odot}$), combining the simulations presented in this work with those of Di Carlo et al. (2019) and Di Carlo et al. (2020b). The maximum mass of merging BBHs is much higher in high-mass YSCs than in low-mass YSCs: the primary mass component is up to $\approx 90 M_{\odot}$ and $\approx 54 M_{\odot}$ in high-mass and low-mass YSCs, respectively. All the systems with primary mass $m_1 > 50 M_{\odot}$ are exchanged BBHs.

Figures 7 and 8 show that, even if we form exchanged BBHs with total mass up to $m_{\text{BBH}} \sim 230 M_{\odot}$ (Figure 6) in the low-mass YSCs, only the least massive systems merge within a Hubble time ($m_{\text{BBH}} < 70 M_{\odot}$). Moreover, the exchanged BBH mergers have similar masses as the original ones. This is very different from what happens in more massive YSCs, where exchanged BBH mergers tend to be more massive than original BBH mergers (Figure 9).

This fundamental difference springs from a number of effects. The first key ingredient is the time at which the dynamical exchange occurs. In low-mass YSCs (Figure 10), most of the exchanged BBHs pair up before the formation of the two BHs (when the binary is still composed of two stars, or of a star and a BH). The time of exchange

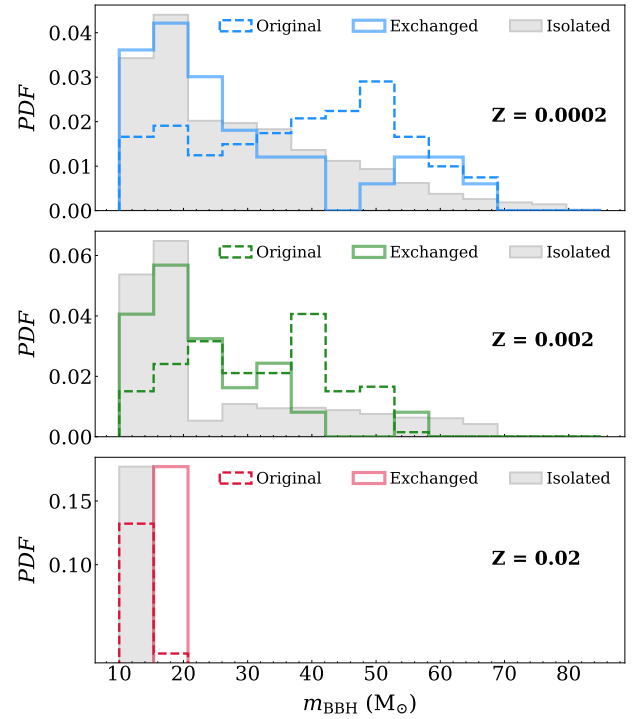


Figure 7. Distribution of total masses ($m_{\text{BBH}} = m_1 + m_2$) of merging BBHs. Solid line: exchanged BBHs; dashed line: original BBHs; grey filled histogram: isolated BBHs. The three plots display, from top to bottom: $Z = 0.0002$, $Z = 0.002$ and $Z = 0.02$.

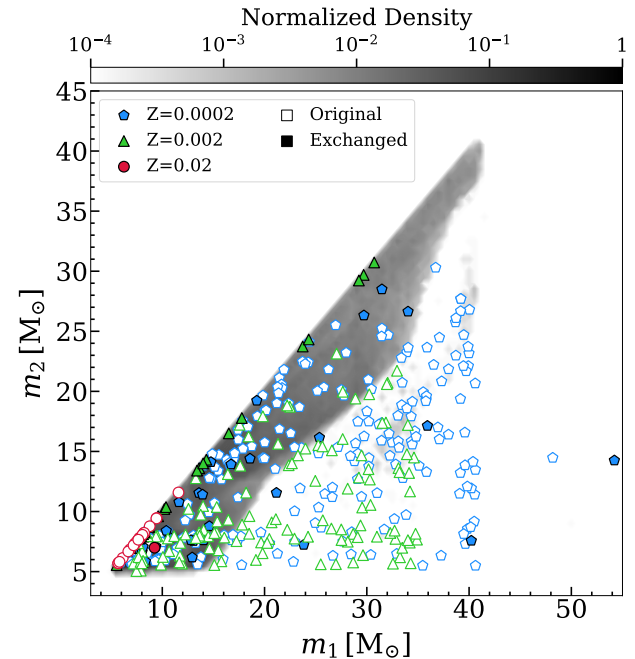


Figure 8. Mass of the primary (m_1) and secondary (m_2) component of merging BBHs in the low-mass YSCs presented in this work. Empty symbols: original BBHs; Filled symbols: exchanged BBHs. Blue: $Z = 0.0002$; green: 0.002 ; red: 0.02 . Filled contours (grey colour map): isolated BBHs mergers for all three metallicities together, from our comparison sample.

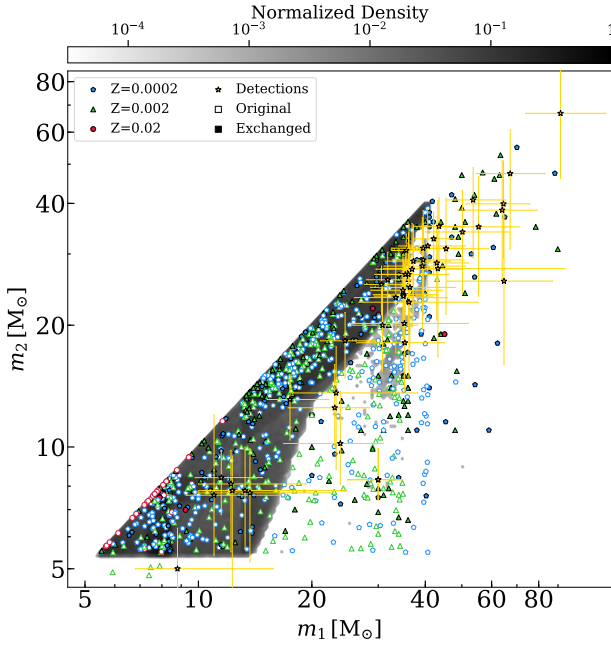


Figure 9. Same as Figure 8 but showing BBHs from both low-mass (this work) and high-mass YSCs (from Di Carlo et al. 2019 and Di Carlo et al. 2020b). The yellow stars indicate all GWTC-2 BBHs (Abbott et al. 2020b). The error bars show the 90% credible interval.

ranges between $5.5 < t_{\text{exch}} < 8$ Myr, while the BBH formation tends to occur later, $6.2 < t_{\text{BBH}} < 10.2$ Myr.

The semi-major axis of the binary system right after the exchange a_{exch} (Figure 10) plays a crucial role: if it is sufficiently small, the exchanged binary undergoes mass transfer and/or common envelope before the formation of the second BH. These processes have two effects. On the one hand, they further shrink the semi-major axis, leaving a binary system that may merge within a Hubble time. On the other hand, they remove a lot of mass from the progenitor stars, leading to the formation of smaller BHs (Linden et al. 2010; Giacobbo & Mapelli 2018). This is apparent from Figure 10, where we see that the smallest BBHs ($m_{\text{BBH}} \sim 20 M_{\odot}$) have the smallest value of a_{exch} but are the result of rather massive binaries.

Finally, the most massive BH progenitors tend to form exchanged binaries with very large values of a_{exch} . This happens because such very massive binaries form via exchange and survive in the lowest-mass YSCs, even if they have a very large semi-major axis: they are hard binaries, even if $a_{\text{exch}} \sim 10^3$ AU. Even if they survive, their semi-major axis is so large that neither binary evolution processes nor further dynamical interactions (which become more and more rare, given the low density of the YSC, Figure 1) can shrink their orbit significantly. For a combination of these effects, exchanged BBH mergers tend to be relatively low mass in low-mass YSCs. In contrast, in more massive star clusters, even the most massive exchanged BBHs have a chance of dynamically shrinking their orbit, till they merge by gravitational wave decay.

Figure 11 shows the distribution of the mass ratios $q = m_2/m_1$ of BBH mergers in low-mass YSCs. Mass ratios of order of one are more common, but the distribution reaches a minimum value $q \approx 0.13$. Mass ratios $q < 0.4$ are orders of magnitude more common in dynamical BBH mergers (both original and exchanged) than isolated binaries. This is an effect of dynamics that can lead to the pairing up of BHs with different masses, especially for exchanged binaries. The chirp mass of merging BBHs ($\mathcal{M} = (m_1 m_2)^{3/5} (m_1 + m_2)^{-1/5}$,

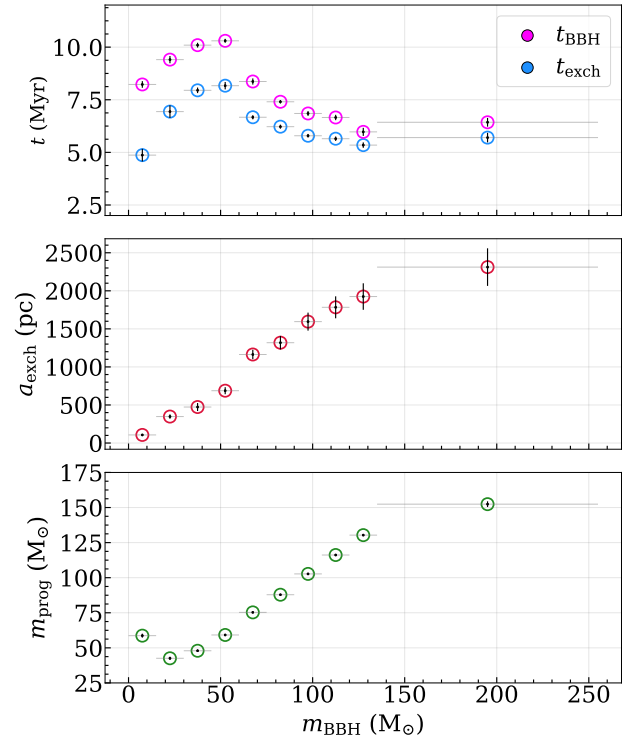


Figure 10. Upper panel: time at which the first exchange occurs (t_{exch} , blue circles) and time at which the second BH in exchanged BBHs forms (t_{BBH} , violet circles) versus the total BBH mass (m_{BBH}) for all the exchanged BBHs with $m_{\text{SC}} \leq 150 M_{\odot}$. Central panel: semi-major axis at time of the exchange (a_{exch}) for all the exchanged BBHs. Lower panel: Total mass of BBH progenitor (m_{prog}) for all exchanged binaries. In all panels, the data point show the median value for all the exchanged BBHs in the same mass bin, while the error bars are obtained with the bootstrap method. BBHs with $m_{\text{SC}} > 150 M_{\odot}$ are shown in a unique large mass bin because of the low statistics in this mass range.

also shown in Figure 11) ranges between a minimum of $\approx 4.7 M_{\odot}$ to a maximum of $\approx 36 M_{\odot}$. Similar to the distribution of total masses, also the one of chirp masses is skewed to lower values for the exchanged than for the original BBHs. Finally, the distribution of delay times t_{delay} (Figure 11) of exchanged, original and isolated BBHs do not show particular differences. The majority of coalescing BBHs merge in $\lesssim 2$ Gyr. All the BBH mergers occur after the binaries have been ejected from the clusters, except for one case in which the BBH merges after ≈ 30 Myr, when is still bound to the cluster.

3.6 BBH Survival Efficiency

Figure 12 shows the BBH survival efficiency (η_s), defined as the number of BBHs that survive in the simulated YSCs at the end of the simulations (N_{BBH}), divided by the total initial SC mass:

$$\eta_s = \frac{N_{\text{BBH}}}{M_*}. \quad (4)$$

We calculate η_s for both our YSCs ($m_{\text{SC}} \in [300, 1000] M_{\odot}$) and those simulated by Di Carlo et al. (2019, 2020b) ($m_{\text{SC}} \in [1000, 30000] M_{\odot}$). We consider both BBHs that will merge in less than a Hubble time and looser BBH systems. The BBH survival efficiency is almost independent of mass in metal-poor YSCs ($Z = 0.0002, 0.002$), showing a weak decrease for large YSC mass. In contrast, metal-rich YSCs show an interesting behaviour: η_s drops

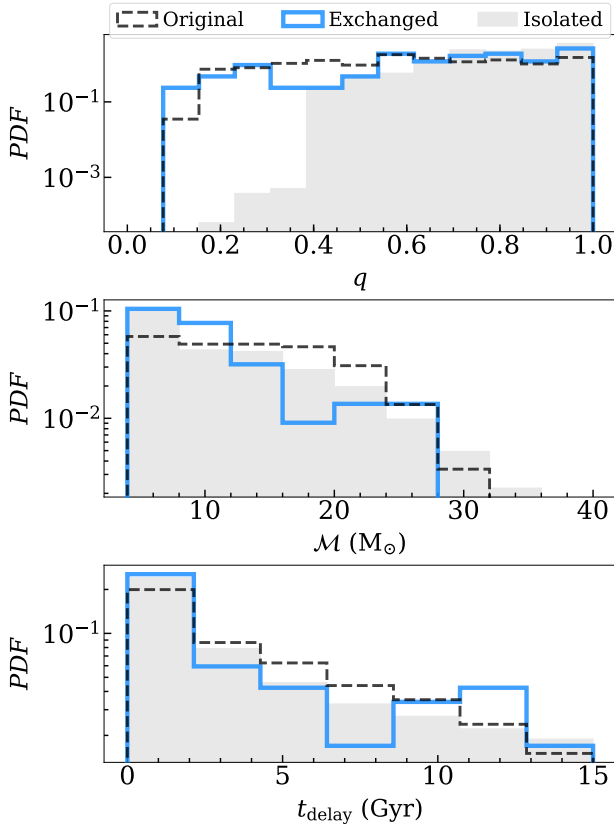


Figure 11. From top to bottom, distribution of mass ratio q , chirp mass M (M_\odot) and delay time t_{delay} (Gyr) of merging BBHs in low-mass YSCs. Black dashed line: original BBHs, blue solid line: exchanged BBHs. Filled grey histograms refer to isolated BBHs. The three metallicities are displayed together.

by a factor of ~ 3 going from low-mass to massive YSCs if we consider the densest star clusters (set A of Di Carlo et al. 2020b), while it remains almost constant if we consider the looser star clusters (set B of Di Carlo et al. 2020b). This indicates that, at solar metallicity, massive binary stars formed in dense stellar systems (set A) are more efficiently disrupted in the higher mass clusters. The same trend does not appear (or mildly appears) at lower metallicity and in looser star clusters (set B). The reason why this behaviour appears only at high metallicity is that BHs produced at $Z = 0.02$ are lighter than those formed in metal-poor YSCs, facilitating the break up of binaries via ionization. In loose star clusters this effect is weaker, because dynamical encounters are less efficient. For example, in massive metal-rich YSCs of set A, no more than 10–15% of the original binaries survive till the end of the simulation (see also Figure 5), while in set B, the surviving binaries are $> 35\%$.

3.7 BBH Merger Efficiency versus Cluster Mass

The merger efficiency, η , is defined as the number of BBH mergers N_{merg} within a Hubble time, divided by the total initial stellar mass of the simulated YSCs:

$$\eta = \frac{N_{\text{merg}}}{M_*} \quad (5)$$

where $M_* = \sum_i m_{\text{SC},i}$, where the index i can run either over all the YSCs simulated at a given metallicity Z , or only over a sub-group of star clusters in the same bin of mass. The merger efficiency is

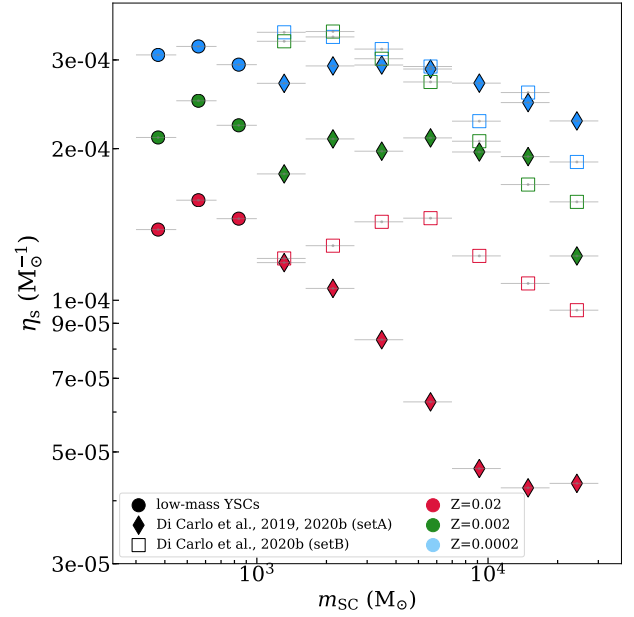


Figure 12. BBH survival efficiency η_s as a function of YSC mass for $Z = 0.0002$ (blue), 0.002 (green) and 0.02 (red). Filled circles refer to the YSCs presented in this work ($m_{\text{SC}} \in [300, 1000] M_\odot$), diamonds refer to set A of Di Carlo et al. 2020b and Di Carlo et al. (2019), while empty squares refer to set B of Di Carlo et al. 2020b. To derive η_s as a function of the cluster mass, we have divided the simulated YSCs in 10 log-spaced mass bins. The error bars are Poissonian uncertainties. The size of each bin is indicated with grey lines along the x-axis.

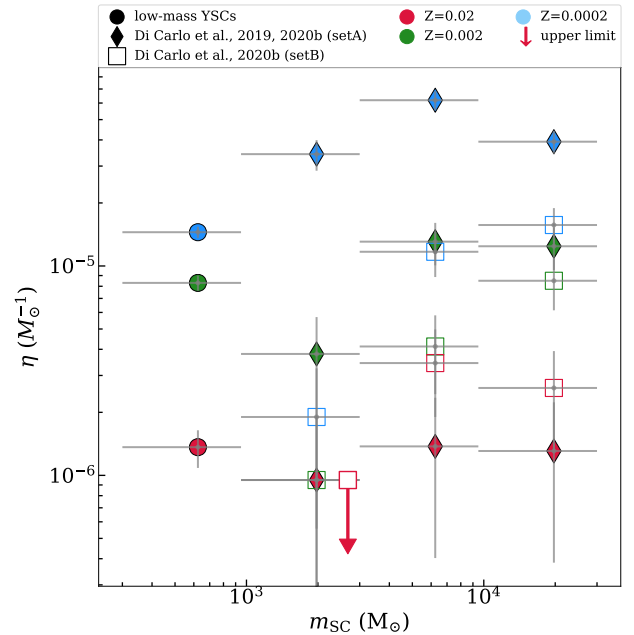


Figure 13. BBHs merger efficiency η of YSCs. Metallicity $Z = 0.0002$ (blue), $Z = 0.002$ (green) and $Z = 0.02$ (red). Filled circles refer to our low-mass YSCs; filled diamonds refer to set A of Di Carlo et al. (2020b) and Di Carlo et al. (2019), while empty squares refer to set B of Di Carlo et al. (2020b). The size of each bin is indicated with grey lines along the x-axis. The red arrow indicates the upper limit of η in the first mass bin for set B. The y-axis grey error bars are uncertainties from Poisson statistics.

Z	η_{SC} [M_{\odot}^{-1}]	η_{IB} [M_{\odot}^{-1}]
0.0002	1.4×10^{-5}	1.3×10^{-4}
0.002	8.3×10^{-6}	2.9×10^{-5}
0.02	1.3×10^{-6}	3.2×10^{-9}

Table 1. Merger efficiency of BBHs for low-mass YSCs and isolated binaries. Column 1: metallicity Z ; column 2: BBH merger efficiency for YSCs η_{SC} ; column 3: BBH merger efficiency for isolated binaries η_{IB} .

a good proxy for the merger rate, because it does not depend on assumptions about the star formation rate and metallicity evolution of the Universe. Here we explore the dependence of the merger efficiency on both m_{SC} and Z .

Figure 13 displays the merger efficiency versus the cluster mass for low-mass YSCs (this work) and high-mass systems studied in Di Carlo et al. (2020b). In general, the merger efficiency of the loose YSCs of set B is smaller than the merger efficiency of the dense YSCs (set A) with the same YSC mass. Thus, in the first approximation, a higher initial stellar density implies a higher merger efficiency.

In the loose YSCs of set B of Di Carlo et al. (2020b), the merger efficiency increases with the cluster mass by about one order of magnitude between $m_{\text{SC}} = 10^3 \text{ M}_{\odot}$ and $3 \times 10^4 \text{ M}_{\odot}$. We see a similar trend for all the considered metallicities, within the Poissonian uncertainties (it may become weaker at $Z = 0.02$, but we have low statistics).

The behaviour of η in the densest YSCs (those presented in this paper plus set A of Di Carlo et al. 2020b) is more varied, depending on the metallicity. At $Z = 0.0002$, η tends to increase with the cluster mass, even if the increase is less steep than for set B. At $Z = 0.002$, η still tends to increase with cluster mass, but the trend is flatter than that for $Z = 0.0002$. Finally, at solar metallicity ($Z = 0.02$), η has a flat trend for low-mass and high-mass dense clusters.

Furthermore, at low metallicity ($Z = 0.0002, 0.002$), the merger efficiency of the dense clusters with $m_{\text{SC}} > 10^4 \text{ M}_{\odot}$ is slightly lower than that of smaller dense YSCs ($m_{\text{SC}} \in [3000, 9500] \text{ M}_{\odot}$). This decrease is a consequence of the higher density, which leads to the break up of more binary stars. In fact, looking at the population of merging BBHs, we find that the percentage of original binaries decreases at higher star cluster mass: original BBH mergers are 85% (75%), 73% (42%) and 53% (42%) of all BBH mergers in the second, third and fourth mass-bin, at $Z=0.0002$ ($Z=0.002$). On the one hand, in most massive YSCs the number of dynamical encounters and thus the formation of new binaries (exchanged BBHs) is significantly enhanced. On the other hand, in such massive systems, encounters may break original binaries, removing a fraction of potential merging BBHs from the systems.

This comparison underlines that star cluster density and star cluster mass are two crucial ingredients for the merger efficiency of BBHs in YSCs. As discussed in Di Carlo et al. (2020b), at low metallicities, where BH masses are higher, dynamical encounters and hardening are more effective in the dense clusters of set A than in the loose clusters of set B.

3.8 Merger Efficiency and Local Merger Rate Density

Table 1 shows the merger efficiency for BBHs from low-mass YSCs (η_{SC}) and from isolated binaries (η_{IB}) at different metallicity.

In metal-poor systems ($Z = 0.0002, 0.002$), the BBH merger efficiency for small YSCs (η_{SC}) is about a factor of ≈ 9 (≈ 4) lower than the BBH merger efficiency for isolated binaries (η_{IB}). This is an

effect of dynamics, that may break up low-mass BBHs (Zevin et al. 2017; Di Carlo et al. 2019) resulting in a lower merger efficiency with respect to isolated binaries.

In contrast, at solar metallicity ($Z = 0.02$) η_{SC} is higher by two orders of magnitude than the η_{IB} . In fact, isolated BBH mergers are extremely rare at solar metallicity, because of the larger efficiency of stellar winds. In fact, the majority of massive stars become Wolf-Rayet stars before they can start a Roche lobe event and do not undergo a common envelope phase: most of the isolated BBHs that form at solar metallicity are too wide to merge within a Hubble time. In contrast, dynamics triggers BBH mergers even in metal-rich YSCs: dynamical encounters lead to the formation of exchanged BBHs and, additionally, gravitational interactions harden existing massive binaries, even in metal-rich systems.

From the merger efficiency, we can estimate the merger rate density in the local Universe as described in Santoliquido et al. (2020, 2021):

$$\mathcal{R}_{\text{BBH}} = \frac{1}{t_{\text{lb}}(z_{\text{loc}})} \int_{z_{\text{max}}}^{z_{\text{loc}}} \psi(z') \frac{dt_{\text{lb}}}{dz'} dz' \times \int_{Z_{\text{min}}(z')}^{Z_{\text{max}}(z')} \eta(Z) \mathcal{F}(z', z_{\text{loc}}, Z) dZ, \quad (6)$$

where $t_{\text{lb}}(z_{\text{loc}})$ is the look-back time evaluated in the local Universe ($z_{\text{loc}} \leq -2.1$), $Z_{\text{min}}(z')$ and $Z_{\text{max}}(z')$ are the minimum and maximum metallicity of stars formed at redshift z' , $\psi(z')$ is the cosmic SFR density at redshift z' (from Madau & Fragos 2017) and $\mathcal{F}(z', z_{\text{loc}}, Z)$ is the fraction of BBHs that form at redshift z' from stars with metallicity Z and merge at redshift z_{loc} normalized to all BBHs that form from stars with metallicity Z . The lookback time t_{lb} is estimated taking the cosmological parameters from Ade et al. (2016). We integrate equation 6 up to redshift $z_{\text{max}} = 15$.

From equation 6 and assuming the metallicity evolution proposed by Madau & Fragos (2017), we obtain a local merger rate density $\mathcal{R}_{\text{BBHs}} = 88^{+34}_{-26} f_{\text{YSC}} \text{ Gpc}^{-3} \text{ yr}^{-1}$, where $f_{\text{YSC}} \in (0, 1]$ is the fraction of the cosmic star formation rate that occurs in YSCs like the ones we simulated. The uncertainty refers to the 50% credible interval and accounts for both star formation rate and metallicity evolution. Calculating the rate for isolated BBHs with the same methodology, we found $\mathcal{R}_{\text{BBHs}} \sim 50 f_{\text{IB}} \text{ Gpc}^{-3} \text{ yr}^{-1}$ (Santoliquido et al. 2020), where $f_{\text{IB}} \in [0, 1]$ is the fraction of the cosmic star formation rate happening in the field. The BBH merger rate density of our low-mass YSCs is similar to the BBH merger rate density of higher mass YSCs, estimated by Di Carlo et al. (2020b) ($\mathcal{R}_{\text{BBHs}} \sim 55 \text{ Gpc}^{-3} \text{ yr}^{-1}$), Banerjee (2021b) ($\mathcal{R}_{\text{BBHs}} \sim 0.5 - 38 \text{ Gpc}^{-3} \text{ yr}^{-1}$) and Kumamoto et al. (2020) ($\sim 70 \text{ Gpc}^{-3} \text{ yr}^{-1}$). It seems unlikely that all the BBH mergers observed by the LVC come from a single formation channel (see, e.g., Abbott et al. 2020d; Zevin et al. 2021; Callister et al. 2020; Wong et al. 2021b; Bouffanais et al. 2021). The LVC recently estimated a BBH merger rate of $\mathcal{R}_{\text{BBHs}} = 52^{+52}_{-26} \text{ Gpc}^{-3} \text{ yr}^{-1}$ and $\mathcal{R}_{\text{BBHs}} = 23.9^{+14.3}_{-8.6} \text{ Gpc}^{-3} \text{ yr}^{-1}$, depending on whether we include or not GW190814 in the BBH population, respectively (Abbott et al. 2020d). When compared to the BBH merger rate density inferred by the LVC, our results suggest that YSCs can give a substantial contribution to the population of BBH mergers in the local Universe.

4 SUMMARY AND CONCLUSIONS

We have studied the formation of BBHs in $\sim 10^5$ low-mass young star clusters ($300 \text{ M}_{\odot} < m_{\text{SC}} < 10^3 \text{ M}_{\odot}$) with different metallicities $Z = 0.02, 0.002$ and 0.0002 , by means of direct N -body simulations. We used the code NBODY6++GPU (Wang et al. 2015) interfaced with

the population-synthesis code MOBSE (Giacobbo et al. 2018). We compare our results with those of high-mass YSCs ($10^3 M_\odot < m_{SC} < 3 \times 10^4 M_\odot$) presented in Di Carlo et al. (2019) and Di Carlo et al. (2020b) and with a sample of isolated binaries evolved with the code MOBSE by Giacobbo & Mapelli (2018).

The lighter YSCs in our sample ($300 < m_{SC} < 700 M_\odot$) tend to over-fill their tidal radius over ≈ 100 Myr and expand more rapidly than the heavier YSCs ($700 < m_{SC} < 1000 M_\odot$) which, in contrast, remain tidally under-filling for the entire simulation. The relaxation time scale of low-mass YSCs is extremely short, $t_{\text{rlx}} \approx \text{few tens of Myr}$. Our clusters are created as already core-collapsed and thus experience a rapid initial expansion of the core radius and an initial drop of the central density (Figure 1).

About 75 – 85% of the BHs formed in our simulations are ejected from their parent cluster because of dynamical recoil. For comparison, only $\sim 35 - 65\%$ of the stars are ejected by the end of the simulation. This difference springs from Spitzer’s instability: the most massive stars (BH progenitors) segregate to the core of the star cluster over a very short timescale (< 1 Myr) in our YSCs. In the core, they undergo dynamical encounters and eject each other, while most of the low-mass stars remain in the loose outskirts of the star cluster.

Focusing on the population of BBHs, we have shown that the typical mass of a BBH does not depend on the cluster mass (Figure 3). We distinguish between original BBHs, which are the result of the evolution of original binary stars, and exchanged BBHs, which form from dynamical exchanges. Exchanged BBHs have median values of the total mass ($m_{\text{BBH}} = m_1 + m_2$) of the order of ~ 80 , ~ 60 and $\sim 20 M_\odot$ at $Z = 0.0002$, 0.002 and 0.02 , respectively. Original BBHs are, on average, less massive (~ 60 , ~ 30 and $\sim 10 M_\odot$ at $Z = 0.0002$, 0.002 and 0.02 , respectively). The masses of original BBHs are more similar to isolated BBHs (Giacobbo et al. 2018) while exchanged BBHs host primary binary components with mass up to $\approx 190 M_\odot$ (Figure 6).

We find that the percentage of exchanged BBHs strongly depends on the star cluster mass: it increases from $\sim 40 - 60\%$ in the lowest-mass YSCs ($300 M_\odot$) up to more than $\approx 75 - 95\%$ in the most massive YSCs ($3 \times 10^4 M_\odot$, from set A of Di Carlo et al. 2020b). The large number of dynamical scatterings in the most massive clusters enhances the probability to form exchanged BBHs and, at the same time, facilitates the ionization of original binaries.

We then focused on the sub-sample of BBHs that reach coalescence in less than a Hubble time. BBH mergers in low-mass YSCs tend to be relatively light, $m_{\text{BBH}} < 70 M_\odot$. About $\approx 90\%$ of merging BBHs are original binaries and most of them (60%) are produced in metal poor environments. Exchanged BBH mergers in low-mass YSCs have masses similar to those of original BBHs. This is very different from what Di Carlo et al. (2020b) found for more massive clusters ($> 10^3 M_\odot$), where exchanged BBH mergers are significantly more massive than original BBH mergers. In low-mass YSCs (Figure 10), most of the exchanged BBHs pair up before the formation of the two BHs: the dynamical exchange involves the progenitor stars. If the binary semi-major axis at time of the exchange is sufficiently tight, the binary experiences mass transfer and/or common envelope before the formation of the second BH, causing mass loss from the progenitor stars that leads to the formation of light BHs. Moreover, very massive BH progenitors tend to form binaries with large semi-major axis ($a \approx 10^3$ AU) that are difficult to shrink through binary evolution processes or dynamical interactions, which become rather rare as the clusters evolve (Figure 1).

Mass ratios $q < 0.4$ are generally more common in dynamical merging BBHs (both original and exchanged BBHs) than in isolated

binaries, because dynamics may pair up BHs with different masses. In low-mass YSCs the majority of coalescing BBHs merge after the binaries have been ejected by the parent clusters before ≈ 2 Gyr.

The BBH survival efficiency η_s , i.e. the number of BBHs that form and survive to the end of the simulation, divided by the total initial star cluster mass, is almost independent of the star cluster mass and central density, especially in metal poor-environments. At solar metallicity, there is a different trend when considering massive dense or loose YSCs (respectively set A and set B of Di Carlo et al. 2020b).

In loose YSCs, the merger efficiency η (i.e. the number of BBH mergers divided by the total initial star cluster mass) increases with the cluster mass by up to one order of magnitude. In dense clusters η and the cluster mass show a very mild correlation in metal poor environments and no correlation at solar metallicity.

At low metallicity ($Z = 0.0002$), the merger efficiency of YSCs is about one order of magnitude lower than that of isolated binaries, because dynamics ejects BHs from the cluster and might break binary systems. In contrast, at $Z = 0.02$, the merger efficiency of YSCs is ~ 400 times higher than that of isolated binaries. In fact, unperturbed binary stars at high metallicity are very difficult to merge, because the progenitor stars become Wolf-Rayet systems (with small stellar radii) and cannot undergo common envelope episodes: their semi-major axis remains too large. In YSCs, dynamics triggers BBH mergers even in metal-rich YSCs. From the merger efficiency (Santoliquido et al. 2020), we estimated a local BBH merger rate density of low-mass YSCs $\mathcal{R}_{\text{BBHs}} = 88^{+34}_{-26} f_{\text{YSC}} \text{ Gpc}^{-3} \text{ yr}^{-1}$, where $f_{\text{YSC}} \in [0, 1]$ is the fraction of the cosmic star formation rate that occurs in YSCs. This result suggests that low-mass YSCs have a significant role in the population of BBH mergers in the local Universe.

ACKNOWLEDGEMENTS

MM, SR, UNDC, GI, AB, NG and FS acknowledge financial support by the European Research Council for the ERC Consolidator grant DEMOBLACK, under contract no. 770017. NG acknowledges financial support by Leverhulme Trust Grant No. RPG-2019-350 and Royal Society Grant No. RGS-R2-202004. We are grateful to Long Wang for his helpful support on NBODY6++GPU. Part of the N -body simulations discussed in this paper were performed at the supercomputer DEMOBLACK at the Physics and Astronomy department “G. Galilei” of the University of Padova, equipped with 192 dual cores, 8 V100 NVIDIA GPUs. We acknowledge the CINECA-INFN agreement, for the availability of high performance computing resources and support.

DATA AVAILABILITY

The data underlying this article will be shared on reasonable request to the corresponding authors.

REFERENCES

- Aarseth S. J., 2003, Gravitational N-Body Simulations
- Aarseth S. J., 2012, *MNRAS*, **422**, 841
- Aasi J., et al., 2015, Classical and Quantum Gravity, **32**, 074001
- Abbott B. P., et al., 2016a, *Physical Review X*, **6**, 041015
- Abbott B. P., et al., 2016b, *Phys. Rev. Lett.*, **116**, 061102
- Abbott B. P., et al., 2016c, *Physical Review Letters*, **116**, 241103
- Abbott B. P., et al., 2019a, *Phys. Rev. X*, **9**, 031040
- Abbott B. P., et al., 2019b, *ApJ*, **882**, L24

- Abbott B. P., et al., 2020a, arXiv e-prints, [p. arXiv:2004.08342](#)
- Abbott R., et al., 2020b, arXiv e-prints, [p. arXiv:2010.14527](#)
- Abbott R., et al., 2020c, arXiv e-prints, [p. arXiv:2010.14529](#)
- Abbott R., et al., 2020d, arXiv e-prints, [p. arXiv:2010.14533](#)
- Abbott R., et al., 2020e, *Phys. Rev. Lett.*, **125**, 101102
- Abbott R., et al., 2020f, *Phys. Rev. Lett.*, **125**, 101102
- Abbott B. P., et al., 2020g, *ApJ*, **892**, L3
- Abbott R., et al., 2020h, *ApJ*, **900**, L13
- Abbott R., et al., 2020i, *ApJ*, **900**, L13
- Acernese F., et al., 2015, *Classical and Quantum Gravity*, **32**, 024001
- Ade P. A. R., Aghanim N., Arnaud M., Lähteenmäki A., Lamarre J. M., Lasenby A., Lattanzi M., 2016, *A&A*, **594**, A13
- Antonini F., Rasio F. A., 2016, *ApJ*, **831**, 187
- Antonini F., Toonen S., Hamers A. S., 2017, *ApJ*, **841**, 77
- Antonini F., Gieles M., Gualandris A., 2019, *MNRAS*, **486**, 5008
- Arca-Sedda M., Capuzzo-Dolcetta R., 2018, *Monthly Notices of the Royal Astronomical Society*, **483**, 152
- Arca-Sedda M., Gualandris A., 2018, *MNRAS*, **477**, 4423
- Arca Sedda M., Mastrobuono-Battisti A., 2019, arXiv e-prints, [p. arXiv:1906.05864](#)
- Arca Sedda M., Mapelli M., Spera M., Benacquista M., Giacobbo N., 2020, *ApJ*, **894**, 133
- Askar A., Szkudlarek M., Gondek-Rosińska D., Giersz M., Bulik T., 2017, *MNRAS*, **464**, L36
- Askar A., Arca Sedda M., Giersz M., 2018, *MNRAS*, **478**, 1844
- Ballone A., Mapelli M., Di Carlo U. N., Torniamenti S., Spera M., Rastello S., 2020, *MNRAS*, **496**, 49
- Banerjee S., 2017, *MNRAS*, **467**, 524
- Banerjee S., 2018, *MNRAS*, **473**, 909
- Banerjee S., 2021a, *MNRAS*, **500**, 3002
- Banerjee S., 2021b, *MNRAS*, **503**, 3371
- Banerjee S., Baumgardt H., Kroupa P., 2010, *MNRAS*, **402**, 371
- Bartos I., Kocsis B., Haiman Z., Márka S., 2017, *ApJ*, **835**, 165
- Bavera S. S., et al., 2021, *A&A*, **647**, A153
- Belczynski K., Kalogera V., Bulik T., 2002, *ApJ*, **572**, 407
- Belczynski K., Kalogera V., Rasio F. A., Taam R. E., Zezas A., Bulik T., Maccarone T. J., Ivanova N., 2008, *ApJS*, **174**, 223
- Belczynski K., Bulik T., Fryer C. L., Ruiter A., Valsecchi F., Vink J. S., Hurley J. R., 2010, *ApJ*, **714**, 1217
- Belczynski K., Holz D. E., Bulik T., O’Shaughnessy R., 2016, *Nature*, **534**, 512
- Belczynski K., et al., 2020, *A&A*, **636**, A104
- Benacquista M. J., Downing J. M. B., 2013, *Living Reviews in Relativity*, **16**, 4
- Bethe H. A., Brown G. E., 1998, *ApJ*, **506**, 780
- Binney J., Tremaine S., 2008, *Galactic Dynamics: Second Edition*. Princeton University Press
- Bouffanais Y., Mapelli M., Gerosa D., Di Carlo U. N., Giacobbo N., Berti E., Baibhav V., 2019, *ApJ*, **886**, 25
- Bouffanais Y., Mapelli M., Santoliquido F., Giacobbo N., Iorio G., Costa G., 2020, arXiv e-prints, [p. arXiv:2010.11220](#)
- Bouffanais Y., Mapelli M., Santoliquido F., Giacobbo N., Di Carlo U. N., Rastello S., Artale M. C., Iorio G., 2021, arXiv e-prints, [p. arXiv:2102.12495](#)
- Callister T. A., Farr W. M., Renzo M., 2020, arXiv e-prints, [p. arXiv:2011.09570](#)
- Casertano S., Hut P., 1985, *ApJ*, **298**, 80
- Chandrasekhar S., 1943, *ApJ*, **97**, 255
- Chen Y., Bressan A., Girardi L., Marigo P., Kong X., Lanza A., 2015, *MNRAS*, **452**, 1068
- Claeys J. S. W., Pols O. R., Izzard R. G., Vink J., Verbunt F. W. M., 2014, *A&A*, **563**, A83
- Di Carlo U. N., Giacobbo N., Mapelli M., Pasquato M., Spera M., Wang L., Haardt F., 2019, *MNRAS*, **487**, 2947
- Di Carlo U. N., Mapelli M., Bouffanais Y., Giacobbo N., Santoliquido F., Bressan A., Spera M., Haardt F., 2020a, *MNRAS*, **497**, 1043
- Di Carlo U. N., et al., 2020b, *MNRAS*, **498**, 495
- Doctor Z., Wysocki D., O’Shaughnessy R., Holz D. E., Farr B., 2020, *ApJ*, **893**, 35
- Dominik M., Belczynski K., Fryer C., Holz D. E., Berti E., Bulik T., Mandel I., O’Shaughnessy R., 2012, *ApJ*, **759**, 52
- Dominik M., Belczynski K., Fryer C., Holz D. E., Berti E., Bulik T., Mandel I., O’Shaughnessy R., 2013, *ApJ*, **779**, 72
- Downing J. M. B., Benacquista M. J., Giersz M., Spurzem R., 2010, *MNRAS*, **407**, 1946
- Farr W. M., Stevenson S., Miller M. C., Mandel I., Farr B., Vecchio A., 2017, *Nature*, **548**, 426
- Fishbach M., Holz D. E., 2020, *ApJ*, **904**, L26
- Fishbach M., Holz D. E., Farr B., 2017, *ApJ*, **840**, L24
- Fragione G., Kocsis B., 2018, *Phys. Rev. Lett.*, **121**, 161103
- Fragione G., Loeb A., 2019a, *MNRAS*, **486**, 4443
- Fragione G., Loeb A., 2019b, *MNRAS*, **490**, 4991
- Fragione G., Leigh N., Ginsburg I., Kocsis B., 2018, arXiv:1806.08385,
- Fragione G., Loeb A., Rasio F. A., 2020, *ApJ*, **895**, L15
- Fryer C. L., Belczynski K., Wiktorowicz G., Dominik M., Kalogera V., Holz D. E., 2012, *ApJ*, **749**, 91
- Fujii M. S., Portegies Zwart S., 2014, *MNRAS*, **439**, 1003
- Fujii M. S., Portegies Zwart S., 2016, *ApJ*, **817**, 4
- Fujii M. S., Tanikawa A., Makino J., 2017, *PASJ*, **69**, 94
- García F., Simaz Bunzel A., Chaty S., Porter E., Chassande-Mottin E., 2021, arXiv e-prints, [p. arXiv:2103.03161](#)
- Gerosa D., Berti E., 2017, *Phys. Rev. D*, **95**, 124046
- Gerosa D., Berti E., O’Shaughnessy R., Belczynski K., Kesden M., Wysocki D., Gladysz W., 2018, *Phys. Rev. D*, **98**, 084036
- Giacobbo N., Mapelli M., 2018, *MNRAS*, **480**, 2011
- Giacobbo N., Mapelli M., 2019, *MNRAS*, **482**, 2234
- Giacobbo N., Mapelli M., Spera M., 2018, *MNRAS*, **474**, 2959
- Goodwin S. P., Whitworth A. P., 2004, *A&A*, **413**, 929
- Goswami S., Kiel P., Rasio F. A., 2014, *ApJ*, **781**, 81
- Gräfenr G., Hamann W.-R., 2008, *A&A*, **482**, 945
- Heggie D. C., 1975, *MNRAS*, **173**, 729
- Hénon M., 1960, *Annales d’Astrophysique*, **23**, 668
- Hills J. G., Fullerton L. W., 1980, *AJ*, **85**, 1281
- Hoang B.-M., Naoz S., Kocsis B., Rasio F. A., Dosopoulou F., 2018, *ApJ*, **856**, 140
- Hurley J. R., Pols O. R., Tout C. A., 2000, *MNRAS*, **315**, 543
- Hurley J. R., Tout C. A., Pols O. R., 2002, *MNRAS*, **329**, 897
- Kimball C., Talbot C., Berry C. P. L., Carney M., Zevin M., Thrane E., Kalogera V., 2020, *ApJ*, **900**, 177
- Kroupa P., 2001, *MNRAS*, **322**, 231
- Kruckow M. U., Tauris T. M., Langer N., Kramer M., Izzard R. G., 2018, *MNRAS*, **481**, 1908
- Kuhn M. A., Hillenbrand L. A., Sills A., Feigelson E. D., Getman K. V., 2019, *ApJ*, **870**, 32
- Kumamoto J., Fujii M. S., Tanikawa A., 2019, *MNRAS*, **486**, 3942
- Kumamoto J., Fujii M. S., Tanikawa A., 2020, *MNRAS*, **495**, 4268
- Küpper A. H. W., Maschberger T., Kroupa P., Baumgardt H., 2011a, *MNRAS*, **417**, 2300
- Küpper A. H. W., Maschberger T., Kroupa P., Baumgardt H., 2011b, *MNRAS*, **417**, 2300
- Lada C. J., Lada E. A., 2003, *ARA&A*, **41**, 57
- Linden T., Kalogera V., Sepinsky J. F., Prestwich A., Zezas A., Gallagher J. S., 2010, *ApJ*, **725**, 1984
- Loeb A., 2016, *ApJ*, **819**, L21
- Madau P., Fragos T., 2017, *ApJ*, **840**, 39
- Makino J., Aarseth S. J., 1992, *PASJ*, **44**, 141
- Mandel I., de Mink S. E., 2016, *MNRAS*, **458**, 2634
- Mapelli M., 2016, *MNRAS*, **459**, 3432
- Mapelli M., Bressan A., 2013, *MNRAS*, **430**, 3120
- Mapelli M., Giacobbo N., 2018, *MNRAS*, **479**, 4391
- Mapelli M., Zampieri L., Ripamonti E., Bressan A., 2013, *MNRAS*, **429**, 2298
- Mapelli M., Giacobbo N., Ripamonti E., Spera M., 2017, *MNRAS*, **472**, 2422
- Mapelli M., Giacobbo N., Santoliquido F., Artale M. C., 2019, *MNRAS*,

- Mapelli M., Spera M., Montanari E., Limongi M., Chieffi A., Giacobbo N., Bressan A., Bouffanais Y., 2020, *ApJ*, **888**, 76
- Mapelli M., et al., 2021, arXiv e-prints, p. [arXiv:2103.05016](#)
- Marchant P., Langer N., Podsiadlowski P., Tauris T. M., Moriya T. J., 2016a, *A&A*, **588**, A50
- Marchant P., Langer N., Podsiadlowski P., Tauris T. M., Moriya T. J., 2016b, *A&A*, **588**, A50
- Marks M., Kroupa P., 2012, *A&A*, **543**, A8
- Marks M., Kroupa P., Dabringhausen J., Pawlowski M. S., 2012, *MNRAS*, **422**, 2246
- McKernan B., Ford K. E. S., Lyra W., Perets H. B., 2012, *MNRAS*, **425**, 460
- McKernan B., et al., 2018, *ApJ*, **866**, 66
- Mennekens N., Vanbeveren D., 2014, *A&A*, **564**, A134
- Mikkola S., Aarseth S. J., 1993, *Celestial Mechanics and Dynamical Astronomy*, **57**, 439
- Miller M. C., Lauburg V. M., 2009, *ApJ*, **692**, 917
- Moe M., Di Stefano R., 2017, VizieR Online Data Catalog, p. [J/ApJ/810/61](#)
- Neijssel C. J., et al., 2019, *MNRAS*, **490**, 3740
- Ng K. K. Y., Vitale S., Farr W. M., Rodriguez C. L., 2020, arXiv e-prints, p. [arXiv:2012.09876](#)
- Nitadori K., Aarseth S. J., 2012, *MNRAS*, **424**, 545
- Nitz A. H., Wang Y.-F., 2021, *Phys. Rev. Lett.*, **126**, 021103
- O’Leary R. M., Kocsis B., Loeb A., 2009, *MNRAS*, **395**, 2127
- Perna R., Wang Y.-H., Farr W. M., Leigh N., Cantiello M., 2019, *ApJ*, **878**, L1
- Peters P. C., 1964, *Physical Review*, **136**, 1224
- Portegies Zwart S. F., McMillan S. L. W., 2000, *ApJ*, **528**, L17
- Portegies Zwart S. F., McMillan S. L. W., 2002, *ApJ*, **576**, 899
- Portegies Zwart S. F., Yungelson L. R., 1998, *A&A*, **332**, 173
- Portegies Zwart S. F., Baumgardt H., Hut P., Makino J., McMillan S. L. W., 2004, *Nature*, **428**, 724
- Portegies Zwart S. F., McMillan S. L. W., Gieles M., 2010, *ARA&A*, **48**, 431
- Rastello S., Amaro-Seoane P., Arca-Sedda M., Capuzzo-Dolcetta R., Fragione G., Tosta e Melo I., 2019, *MNRAS*, **483**, 1233
- Rastello S., Mapelli M., Di Carlo U. N., Giacobbo N., Santoliquido F., Spera M., Ballone A., Iorio G., 2020a, *MNRAS*, **497**, 1563
- Rastello S., Carraro G., Capuzzo-Dolcetta R., 2020b, *ApJ*, **896**, 152
- Rodriguez C. L., Morscher M., Pattabiraman B., Chatterjee S., Haster C.-J., Rasio F. A., 2015, *Physical Review Letters*, **115**, 051101
- Rodriguez C. L., Chatterjee S., Rasio F. A., 2016a, *Phys. Rev. D*, **93**, 084029
- Rodriguez C. L., Zevin M., Pankow C., Kalogera V., Rasio F. A., 2016b, *ApJ*, **832**, L2
- Rodriguez C. L., Amaro-Seoane P., Chatterjee S., Kremer K., Rasio F. A., Samsing J., Ye C. S., Zevin M., 2018, *Phys. Rev. D*, **98**, 123005
- Rodriguez C. L., Zevin M., Amaro-Seoane P., Chatterjee S., Kremer K., Rasio F. A., Ye C. S., 2019, *Phys. Rev. D*, **100**, 043027
- Samsing J., 2018, *Phys. Rev. D*, **97**, 103014
- Samsing J., D’Orazio D. J., 2018, *MNRAS*, **481**, 5445
- Samsing J., Askar A., Giersz M., 2018, *ApJ*, **855**, 124
- Sana H., et al., 2012, *Science*, **337**, 444
- Sánchez N., Alfaro E. J., 2009, *ApJ*, **696**, 2086
- Santoliquido F., Mapelli M., Bouffanais Y., Giacobbo N., Di Carlo U. N., Rastello S., Artale M. C., Ballone A., 2020, *ApJ*, **898**, 152
- Santoliquido F., Mapelli M., Giacobbo N., Bouffanais Y., Artale M. C., 2021, *MNRAS*, **502**, 4877
- Silsbee K., Tremaine S., 2017, *ApJ*, **836**, 39
- Spera M., Mapelli M., 2017, *MNRAS*, **470**, 4739
- Spera M., Mapelli M., Giacobbo N., Trani A. A., Bressan A., Costa G., 2019, *MNRAS*, **485**, 889
- Spitzer L., 1987a, Dynamical evolution of globular clusters
- Spitzer L., 1987b, Dynamical evolution of globular clusters
- Stegmann J., Antonini F., 2021, *Phys. Rev. D*, **103**, 063007
- Stevenson S., Berry C. P. L., Mandel I., 2017, *MNRAS*, **471**, 2801
- Stiefel E., 1965, *Journal für die reine und angewandte Mathematik*, **218**, 204
- Stone N. C., Metzger B. D., Haiman Z., 2017, *MNRAS*, **464**, 946
- Tagawa H., Haiman Z., Kocsis B., 2020, *ApJ*, **898**, 25
- Tang P. N., Eldridge J. J., Stanway E. R., Bray J. C., 2020, *MNRAS*, **493**, L6
- Trani A. A., Mapelli M., Bressan A., 2014, *MNRAS*, **445**, 1967
- Tutukov A., Yungelson L., 1973, *Nauchnye Informatsii*, **27**, 70
- VanLandingham J. H., Miller M. C., Hamilton D. P., Richardson D. C., 2016, *ApJ*, **828**, 77
- Vitale S., Lynch R., Sturani R., Graff P., 2017, *Classical and Quantum Gravity*, **34**, 03LT01
- Wang L., Spurzem R., Aarseth S., Nitadori K., Berczik P., Kouwenhoven M. B. N., Naab T., 2015, *MNRAS*, **450**, 4070
- Wang L., et al., 2016, *MNRAS*, **458**, 1450
- Webbink R. F., 1984, *ApJ*, **277**, 355
- Wong K. W. K., Gerosa D., 2019, *Phys. Rev. D*, **100**, 083015
- Wong K. W. K., Breivik K., Kremer K., Callister T., 2021a, *Phys. Rev. D*, **103**, 083021
- Wong K. W. K., Breivik K., Kremer K., Callister T., 2021b, *Phys. Rev. D*, **103**, 083021
- Yang Y., Bartos I., Haiman Z., Kocsis B., Márka Z., Stone N. C., Márka S., 2019, *ApJ*, **876**, 122
- Ye C. S., Fong W.-f., Kremer K., Rodriguez C. L., Chatterjee S., Fragione G., Rasio F. A., 2020, *ApJ*, **888**, L10
- Zevin M., Pankow C., Rodriguez C. L., Sampson L., Chase E., Kalogera V., Rasio F. A., 2017, *ApJ*, **846**, 82
- Zevin M., Samsing J., Rodriguez C., Haster C.-J., Ramirez-Ruiz E., 2019, *ApJ*, **871**, 91
- Zevin M., et al., 2020, arXiv e-prints, p. [arXiv:2011.10057](#)
- Zevin M., et al., 2021, *ApJ*, **910**, 152
- Ziosi B. M., Mapelli M., Branchesi M., Tormen G., 2014, *MNRAS*, **441**, 3703
- de Mink S. E., Mandel I., 2016a, *MNRAS*, **460**, 3545
- de Mink S. E., Mandel I., 2016b, *MNRAS*, **460**, 3545
- du Buisson L., et al., 2020, *MNRAS*, **499**, 5941